Spanning the Flow Regimes: Generic Fluidized-Bed Reactor Model

I. A. Abba, J. R. Grace, and H. T. Bi
Fluidization Research Center, Dept. of Chemical and Biological Engineering, University of British Columbia, Vancouver, BC, Canada, V6T 1Z4

M. L. Thompson
Procter and Gamble, Cincinnati, OH 45201

Probabilistic averaging is used to model fluidized-bed reactors across the three fluidization flow regimes most commonly encountered in industry (bubbling, turbulent, and fast fluidization), extending earlier work, which introduced this approach to bridge the bubbling and turbulent regimes of fluidization. In extending this concept to the fast fluidization regime, the probabilities of being in each of the three regimes are represented as probability density functions derived from regime boundary transition data. The three regime-specific models — a generalized version of a two-phase bubbling bed model at low gas velocities, a dispersed flow model for turbulent beds at intermediate velocities, and a generalized version of a core-annulus model at higher velocities — are employed, leading to improved predictions compared with any of the individual models, while avoiding discontinuities at the regime boundaries. Predictions from the new integrated model are in good agreement with available ozone decomposition data over the full range of applicability covered elsewhere.

Introduction

Gas-fluidized-bed reactors are widely used in industry for catalytic reactions (such as catalytic cracking, acrylonitrile production, and chlorination reactions) and for gas-solid reactions (such as combustion, gasification, and ore roasting). In each case, a commercial reactor can be operated in three flow regimes—bubbling, turbulent or fast fluidization. The bubbling and fast fluidization regimes have been extensively studied. Models for the bubbling regime generally consider at least two "phases," a dilute phase representing the bubbles and a continuous or dense phase. The solid fractions, mixing parameters and interchange between phases need to be specified. Bubbling bed models, such as the Kunii and Levenspiel (1969) three-phase model and the Grace (1984) two-phase model, have been successful in simulating the bubbling bed phenomena with proper estimation of bubble size. The turbulent regime has been studied less than the other two regimes considered in this work (see Bi et al. (2000) for a recent review). Some models assume single-phase one-dimensional (1-D) plug flow (for example, Fane and Wen, 1982), while others adopt axially dispersed plug flow (Edwards and Avidan, 1986; Foka et al., 1996). The latter approach has been successful in modeling fully turbulent fluidization. Single-region 1-D models and two-region models with and without allowance for hydrodynamic axial gradients have been considered for the fast fluidization regime (Grace and Lim, 1997). Single-region models have generally been unsuccessful, as they do not accurately portray the behavior in CFB reactors. Two-region models are more realistic, as there is ample evidence that distinct dilute core and dense annular regions exist. Some of these two-region models ignore axial gradients (for example, Brereton et al., 1988), while others allow for axial gradients (for example, Puchyr et al., 1997).

Until recently, each of these flow regimes was treated separately with a distinct reactor model. The implicit assumption has been that the flow regime is known with certainty for given operating conditions and particle properties. This results in substantial discontinuities at the boundaries between the flow regimes, notwithstanding the fact that the transitions tend to be diffuse and gradual in nature, with a continuous

Correspondence concerning this article should be addressed to J. R. Grace.
Current address of I. A. Abba: SABIC R&T, Riyadh 11552, Saudi Arabia.

variation in reactor performance as one passes from one flow regime to another (for example, Sun, 1991). Most commercially important catalytic processes (such as acrylonitrile, phthalic anhydride, oxy-chlorination, and so on) operate between the bubbling-turbulent and turbulent-fast fluidization regimes (Bolthrunis, 1989; Rhodes, 1996). A turbulent fluidized bed possesses aspects of both bubbling beds, where the mass-transfer resistance between the bubble and dense phases affects conversion and selectivity, and fast-fluidized beds, where there is relatively rapid interchange between the dilute core and the dense annular region containing most of the particles. In addition, there is considerable uncertainty in the flow regime transition correlations. Various methods have been used to determine the transition velocities U_c and U_{se}, and different methods tend to give different results. In spite of the many studies on the criteria for transition to different flow regimes, they have not yet been established with certainty (Bi et al., 2000).

In earlier work (Thompson et al., 1999; Grace et al., 1999), we introduced a "Generalized Bubbling Turbulent" (GBT) model based on the probabilistic averaging approach. This model provides a smooth transition between the first two of the three principal flow regimes and gives good agreement with available data for low and intermediate gas velocities. In this article, we extend this approach so that the new version of the model (which we call the "Generic Fluidized Bed Reactor" (or GFBR) model) provides a seamless way of covering the complete range of gas velocities and flow conditions from minimum bubbling right up to fully fast fluidization conditions. The goals are to overcome the difficulties in predicting the transition boundaries among the three flow regimes and to eliminate discontinuities at the boundaries, while giving improved predictions of particle and gas dynamics and reactor performance.

GFBR Model

Our approach involves formulation of model equations that describe phenomena within each of the three flow regimes, while providing smooth transitions between them, normally without complete certainty of being in any regime. This enables prediction of reactor performance for the three regimes through weighted averaging of the three regime-specific models themselves (not of their predictions). The generalized model is shown in Figure 1. As in Thompson et al. (1999), we

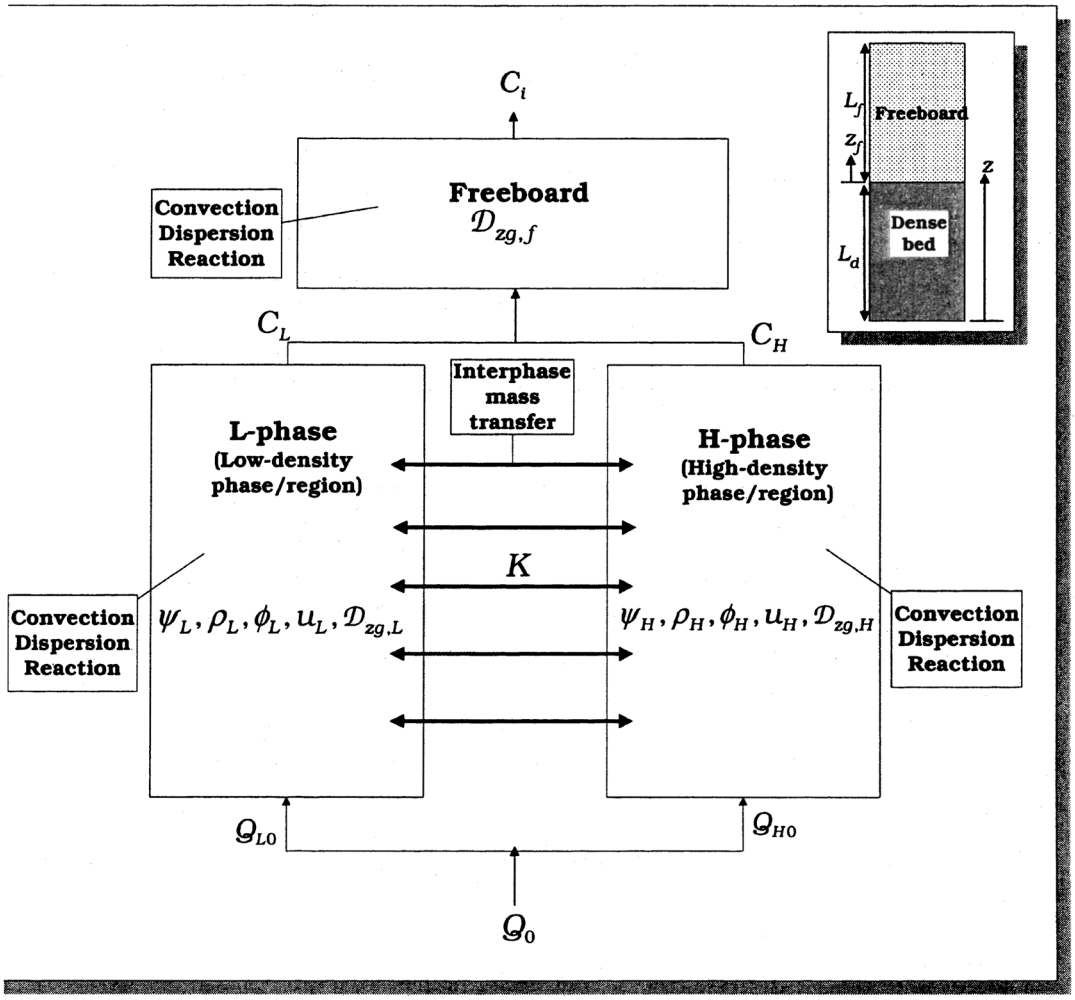

Figure 1. Generalized 1-D, two-phase/region model with freeboard.

Inset shows axial notations for the two regions.

use for the dilute phase/region the general descriptor "low-density" (L) phase and for the dense phase/region "high-density" (H) phase. Thus, for the three principal flow regimes under consideration, the L-phase represents the bubble phase at low U and the core region at high U, while the H-phase represents dense/emulsion phase at low U and the outer annular region at high U.

Dense Bed

From the various reactor models written specifically for the three fluidization flow regimes, three regime-specific models are chosen to represent the limiting behavior of the GFBR model corresponding to fully bubbling, turbulent, and fast fluidization conditions: (i) the generalized version of the Grace (1984) two-phase bubbling bed model (expanded to include dispersion in both phases) at low gas velocities; (ii) the dispersed flow model for turbulent beds at intermediate velocities; (iii) a generalized version of the Brereton et al. (1988) core-annulus model (expanded to include reaction terms, as well as dispersion terms in both the core and annulus regions) at higher velocities. These regime-specific models are chosen because they are realistic and have had some success in describing the physical phenomena in the individual flow regimes. In addition, after incorporating these generalizations, they become fully compatible with each other, and, therefore, a single model formulation each for the L and H-phase can describe all three flow regimes.

Mole balance for the two-phases/regions

Steady-state two-phase/region mole balances represent the two-phase bubbling bed model in the low velocity limit, dispersed flow model at intermediate gas velocities where the turbulent fluidization regime is predominant, and the core-annulus model in the high velocity limit

$$\psi_L u_L \frac{\partial C_{iL}}{\partial z} - \psi_L D_{zg,L} \frac{\partial^2 C_{iL}}{\partial z^2} - \frac{\psi_L D_{rg,L}}{r} \frac{\partial}{\partial r}\left(r \frac{\partial C_{iL}}{\partial r}\right) + k_{LH} a_I \psi_L (C_{iL} - C_{iH}) + \psi_L \rho_L \text{Rate}_{iL} = 0 \quad (1)$$

$$\psi_H u_H \frac{\partial C_{iH}}{\partial z} - \psi_H D_{zg,H} \frac{\partial^2 C_{iH}}{\partial z^2} - \frac{\psi_H D_{rg,H}}{r} \frac{\partial}{\partial r}\left(r \frac{\partial C_{iH}}{\partial r}\right) + k_{LH} a_I \psi_L (C_{iH} - C_{iL}) + \psi_H \rho_H \text{Rate}_{iH} = 0 \quad (2)$$

Overall balances

$$C_i = q_L C_{iL} + q_H C_{iH} \quad (3)$$

The boundary conditions are

$$\text{at } z = 0 \quad -D_{zg,L} \frac{\partial C_{iL}}{\partial z} = u_L \left(C_{iL}\big|_{o-} - C_{iL}\big|_{o+}\right)$$

$$-D_{zg,H} \frac{\partial C_{iH}}{\partial z} = u_H \left(C_{iH}\big|_{o-} - C_{iH}\big|_{o+}\right) \quad (4)$$

$$\text{at } z = L \quad \frac{\partial C_{iL}}{\partial z} = 0, \qquad \frac{\partial C_{iH}}{\partial z} = 0 \quad (5)$$

$$\text{at } r = 0 \quad \frac{\partial C_{iL}}{\partial r} = 0, \qquad \frac{\partial C_{iH}}{\partial r} = 0 \quad (6)$$

$$\text{at } r = R \quad \frac{\partial C_{iL}}{\partial r} = 0, \qquad \frac{\partial C_{iH}}{\partial r} = 0 \quad (7)$$

The net rate of consumption of component i in the jth phase participating in N_r reactions can be written

$$\text{Rate}_i = \sum_{k=1}^{N_r} \nu_{ik} r_k(C)|_j$$

where the stoichiometric coefficients ν_{ik} are positive for products, negative for reactants, and zero for nonreacting species.

Energy balance

The steady-state energy balance equation for the fluid-bed reactor with cooling can be written (neglecting any temperature differences between the L- and H-phases at a given level)

$$\frac{d}{dz}\left(k_e \frac{dT}{dz}\right) - C_{pg} \rho_g U \frac{dT}{dz} + \phi \sum_k^{N_r} (\Delta H_{k,i=base\ rxt} \times \text{Rate}_{i=base\ rxt}) - hA_s (T - T_{\text{cool}}) = 0 \quad (8)$$

with corresponding boundary conditions

$$\text{at } z = 0 \quad -k_e \frac{dT}{dz} = UA \rho_g C_{pg} (T_o - T) \quad (9)$$

$$\text{at } z = L \quad \frac{dT}{dz} = 0 \quad (10)$$

Pressure balance

The pressure, assuming the only contribution to the axial pressure drop is the hydrostatic head of solids (that is, ignoring accelerational effects and friction at the walls), is given by

$$-\frac{dP}{dz} = \rho_p g (1 - \epsilon) \quad (11)$$

The boundary condition at $z = 0$ is

$$P = P_o \quad (12)$$

Freeboard Region

Accounting for the freeboard is also important in extending the probabilistic modeling approach to the fast fluidization regime. The height of integration must be extended to cover the total column/reactor height.

Consider the dense and freeboard regions shown in Figure 1. The solids concentration in the freeboard is assumed to decay exponentially according to (Kunii and Levenspiel, 1991)

$$\phi = \phi^* + (\phi_d - \phi^*) e^{-a z_f} \quad (13)$$

where z_f is the freeboard axial coordinate. The saturation carrying capacity ϕ^* is obtained from

$$\phi^* = \text{MIN}(\phi_1^*, \phi_2^*) \tag{14}$$

where the value for low and intermediate velocities ϕ_1^* is correlated (Morikawa et al., 2001) by

$$\phi_1^* = 0.022(U - U_{mb})^{3.64} \tag{15}$$

while, at high gas velocities, ϕ_2^* can be obtained (assuming $v_t \ll U$) from

$$\phi_2^* = G_s/\rho_p(U - v_t) \tag{16}$$

where the terminal velocity v_t is calculated assuming particles of the same size as in the bed. The net solids circulation flux G_s is obtained by weighting with the respective regime probabilities the solids entrainment E_∞ (Choi et al., 1998) at low and intermediate superficial velocities, and the average solids flux G_{so} in the high velocity limit so that

$$G_s = E_\infty(1 - P_{\text{fast}}) + G_{\text{so}} P_{\text{fast}} \tag{17}$$

where P_{fast} is the probability of being in the fast fluidization regime, described in detail below. The product of the decay constant a and the gas velocity U has been found to be a constant (Kunii and Levenspiel, 1991, 1997). For group A and B particles, a value of "3" reasonably fits measured solids concentration for a wide range of freeboard data pooled by Kunii and Levenspiel (1991). A slightly modified form of the relation is

$$a = \frac{3}{(U - U_{mf})} \tag{18}$$

The total solids inventory in the column is

$$M_s = A\rho_p\left(L_d\phi_d + L_f\overline{\phi}_f\right) \tag{19}$$

where $\overline{\phi}_f$ is the average holdup of solids in the freeboard given by

$$\overline{\phi}_f = \frac{1}{L_f}\int_0^{L_f}\phi dz_f = \phi^* + \frac{\phi_d - \left(\phi^* + (\phi_d - \phi^*)e^{-aL_f}\right)}{aL_f} \tag{20}$$

The freeboard and dense bed heights are obtained by iteratively solving Eqs. 19 and 20, noting that $L_t = L_d + L_f$. The freeboard region is then modeled as being in axially dispersed plug flow with

$$D_{zg,f} = 0.195\left(1 - \overline{\phi}_f\right)^{-4.12} \tag{21}$$

from the correlation of Li and Wu (1991).

Table 1. Summary of Bed and Phase Balances

Phase volume allocation	$\psi_L + \psi_H = 1$
Phase gas holdup allocation	$\epsilon = \psi_L\epsilon_L + \psi_H\epsilon_H$
Phase velocity allocation	$U = \psi_L u_L + \psi_H u_H$
Phase density allocation	$\rho = \psi_L\rho_L + \psi_H\rho_H$
L-phase volume allocation	$\epsilon_L + \phi_L = 1$
H-phase volume allocation	$\epsilon_H + \phi_H = 1$
Bed volume allocation	$\epsilon + \phi = 1$
Phase dispersion distribution	$D = \psi_L D_{zg,L} + \psi_H D_{zg,H}$

Bed and Phase Balances

Phase balances relate only to the dense region where there are two distinct phases, while bed material balances apply to the entire column. Table 1 summarizes the pertinent balances.

Representing the Regime Boundaries and Quantifying their Uncertainty

The probabilities of being above or below the regime transition boundaries are computed by imposing appropriate probability density functions, using the U_c and U_{se} regime boundary correlations and the uncertainty associated with them. These probabilities are then used as proxies for the probabilities of the applicability of the regime-specific models in the different flow regimes. Note that, when dealing with multiple models, the point prediction with minimum variance in prediction errors is their probabilistic average (Lainiotis, 1971; Thompson, 1996; Murray-Smith and Johanssen, 1997). Let:

- $p_i(U|\text{Ar})$ = probability density function (pdf) representing the uncertainty in the regime correlation for U_i (where subscript "i" is used to denote either "c" or "se").
- P_{bubb}, P_{turb}, P_{fast} = probabilities of being in the bubbling, turbulent, and fast fluidization flow regimes, respectively, with the sum always equal to 1.

The gamma probability density function has been determined to be the most appropriate pdf satisfying all the constraints: uncertainty/error "e_i" in correlations normally distributed with mean "0", variances σ_i^2 and $U_{se} > U_c > 0$ (Thompson, 1996; Thompson et al., 1999). If the transition velocity U_i is far enough from zero, the pdfs can also be assumed to be normally distributed with the same means and variances. For example, the uncertainty in the regime correlation for U_{se} can be represented by the Gaussian pdf

$$p_{se}(U|\text{Ar}) = \frac{1}{\sigma_{se}\sqrt{2\pi}}\exp\left(-\frac{(U - U_{se})^2}{2\sigma_{se}^2}\right) \tag{22}$$

For ease of computation, sigmoid-shaped logistic regression functions (LRFs) were fitted to the cumulative distributions evaluated from the Gaussian function

$$P_{\text{fast}} = P(U > U_{se}) = (1 + e^{-\beta v_{se}})^{-1} \equiv \int_U^\infty p_{se}(U|\text{Ar})dU \tag{23}$$

where

$$v_{se} = \frac{(U - U_{se})}{\sigma_{se}} \tag{24}$$

Table 2. Summary of Correlations for Regime Transition Velocities

Source	Regime Boundary Correlation	Normalized Standard Deviation
Bi and Grace (1995)	$Re_c = 0.57\ \mathrm{Ar}^{0.46}$	$\sigma_c^* = 0.36$
	$Re_{se} = 1.53\ \mathrm{Ar}^{0.5}$	$\sigma_{se}^* = 0.52$
This work	$Re_c = 0.74\ \mathrm{Ar}^{0.426}$	$\sigma_c^* = 0.29$
This work	$Re_{se} = 1.68\ \mathrm{Ar}^{0.469}$	$\sigma_{se}^* = 0.45$

It was found that $\beta = 1.7$ fitted both the Gaussian and gamma distributions within a 1% tolerance. Complete assignment of all the probabilities is specified below.

In constructing the regime probability diagram for our probabilistic approach, we need to specify some minimum $U = U_{\min}$ below which there is zero probability of turbulent fluidization. To ensure this, we impose the following constraint: for U just above U_{mb} ($U_{mb} < U < U_{\min}$), P_{bubb} must be 1 and $P_{\text{turb}} = P_{\text{fast}} = 0$. $U_{\min}$ was assigned as $U_{\min} = 2U_{mb}$ or $U_c/10$, whichever is lower. The same problem could arise with respect to some minimum velocity below which the bed has 0 probability of being in the fast fluidization regime, such as to avoid the coexistence of bubbling and fast fluidization conditions. However, given that the mean of the U_{se} distribution is well above zero, it was not necessary to impose a further constraint on the lower limit of U where P_{fast} is nonzero. Overall, the set of constraints $U_{se} > U_c > U_{\min} > U_{mb} > 0$ was satisfied in all cases.

Central to the probability predictions in the GFBR model is a reliable estimate of the standard deviation of the error σ_i. In earlier work (Thompson et al., 1999), a reasonable value of 0.2 m/s was adopted for σ_c and the need to estimate this parameter from actual hydrodynamic data was noted. With the aid of the raw data used to determine the flow regime transition correlations for U_c and U_{se} (Bi et al., 1995) and additional data (Bi, 1994), improved correlations have been developed here with a reduced level of dispersion. Estimates of the normalized standard deviations σ_i^* at the regime boundary correlations are summarized in Table 2. Note that σ_i^* is assumed to be independent of operating conditions and particle properties. With these controls and by invoking the axioms of probability theory, the probabilities of being in each of the three flow regimes are expressed as

$$P_{\text{bubb}} = 1 - P(U^* > U_c^*) = 1 - \left[1 + e^{-\beta v_c^*}\right]^{-1} \quad (25)$$

$$P_{\text{fast}} = P(U^* > U_{se}^*) = \left[1 + e^{-\beta v_{se}^*}\right]^{-1} \quad (26)$$

and from the summation rule

$$P_{\text{turb}} = 1 - P_{\text{fast}} - P_{\text{bubb}} \quad (27)$$

where

$$U_c^* = Re_c/\mathrm{Ar}^{1/3};\ v_c^* = \frac{(U^* - U_{\min}^*) - U_c^*}{\sigma_c^*};$$

$$\sigma_c^{*2} = \frac{1}{n-1}\sum_{j=1}^{n}\left[U_{c,\exp,j}^* - U_c^*(\mathrm{Ar})_j\right]^2 \quad (28)$$

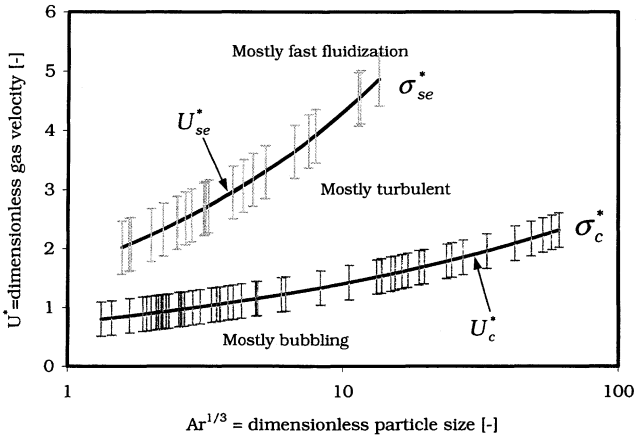

Figure 2. Regime diagram boundaries and regions of uncertainty.

Correlations lines are from Table 2.

$$U_{se}^* = Re_{se}/\mathrm{Ar}^{1/3};\ v_{se}^* = \frac{U^* - U_{se}^*}{\sigma_{se}^*};$$

$$\sigma_{se}^{*2} = \frac{1}{n-1}\sum_{j=1}^{n}\left[U_{se,\exp,j}^* - U_{se}^*(\mathrm{Ar})_j\right]^2 \quad (29)$$

Figure 2 shows regions of uncertainty in the correlations for U_c^* and U_{se}^* depicted by error bars (corresponding to $2\sigma_i^*$ in the correlations). Figure 3a plots the pdfs representing the uncertainties in the regime transition correlations. The corresponding probabilities of operating within each of the three flow regimes appear in Figure 3b for $\mathrm{Ar} = 10$. As expected, bubbling conditions dominate for low U, turbulent conditions at intermediate U, and fast fluidization at large U, with smooth transitions in between.

Flow Regime Transition Equations

With the probabilities of being in each flow regime determined, the next critical step is to use these probabilities as weighting factors to obtain point estimates of the hydrodynamic parameters. The model parameters (coefficients in the mole and energy balance equations for each separate fluidization regime) are then weighted according to

$$\hat{\theta} = \sum_{j=1}^{3}\theta_j P_j \quad (30)$$

where θ_j is the value of θ for regime j and P_j is the probability of being in regime j with $j = 1$ for bubbling fluidization, 2 for turbulent fluidization, and 3 for fast fluidization. For example, the point estimate $\hat{\epsilon}$ from the expected values of ϵ in each regime is obtained as

$$\hat{\epsilon} = \epsilon_{\text{bubb}} P_{\text{bubb}} + \epsilon_{\text{turb}} P_{\text{turb}} + \epsilon_{\text{fast}} P_{\text{fast}} \quad (31)$$

where ϵ_{bubb}, ϵ_{turb}, and ϵ_{fast} are the voidages in the bubbling, turbulent, and fast fluidization flow regimes given in Table 3; this table also lists the equations used to evaluate all the av-

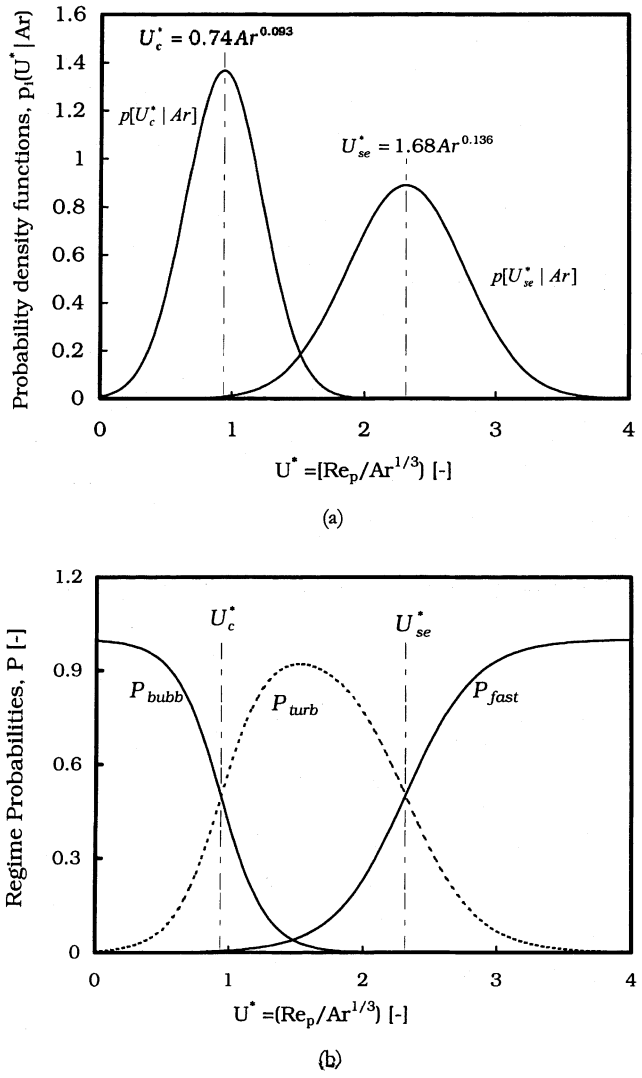

Figure 3. (a) Uncertainties in flow regime boundary correlations; (b) probability of being in each regime as a function of dimensionless superficial gas velocity (Ar = 10).

eraged variables in the three flow regimes. The equations employed to estimate other hydrodynamic parameters such as u_{br}, d_b, and r_C for each of the three regimes, and for required thermophysical properties such as gas mixture diffusivity, are given in Abba (2001). Note that it will be straightforward to replace the correlations or mechanistic equations currently in use by better ones as these become available through future work.

The complete steps in the probabilistic approach to GFBR modeling can be summarized as follows: (a) Generalized model equations based on mole, energy, and pressure balances are formulated applicable over the fluidization regimes of interest; (b) the uncertain regime boundaries are represented as probability density functions (pdfs) using appropriate distributions; (c) the probability of being in regime j is determined given the operating conditions and model parameters ($P(H = H_j|x)$); (d) the hydrodynamic parameters (transition variables) pertaining to each flow regime and needed by the model are calculated; (e) the transition parameters are weighted and averaged as shown in Eqs. 30 and 31; (f) finally, the differential equations posed in step (a) with the weighted coefficients now provided are solved with the boundary conditions to obtain the concentrations, temperature, and pressure as functions of axial coordinate z along the entire reactor and at the exit.

Limits of GFBR Model

The model is explicitly developed to span the three principal fluidization flow regimes. While it would be possible to extend this model to other flow regimes such as slug flow or dilute pneumatic conveying, its applicability is currently limited to bubbling, turbulent, and fast fluidization conditions and transitions between them. Therefore, we note the following limits of the model:

(a) $U > U_{mb}$, that is, the gas velocity is at least sufficient to initiate bubbling;

(b) A large or shallow enough column and/or small enough particles that slug flow conditions are avoided over the entire range of interest;

(c) $U < U_{CA}$ or $G_s > G_{s,CA}$ (Grace and Bi, 1997) in the high gas velocity limit to avoid the dilute-phase transport flow regime;

(d) $U < U_{DSU} = 0.0113 G_s^{1.192} \rho_g^{-1.064} [\mu g(\rho_p - \rho_g)]^{-0.064}$ to ensure that the system is not operating in the dense suspension upflow regime (Grace et al., 1999).

As in our earlier work (Thompson et al., 1999; Grace et al., 1999), the probabilistic model was solved using gPROMS software from Process Systems Enterprise Limited. Full details are given by Abba (2001).

Application to Ozone Decomposition Data

The capability of the model in eliminating discontinuities at the boundaries, while giving improved predictions of particle and gas dynamics and of reactor performance, is demonstrated using experimental ozone decomposition data from Sun (1991) (see also Sun and Grace, 1990; Grace and Sun, 1991), covering a wide range of superficial gas velocities and catalyst activities. No other data reported in the literature cover such an extensive range of gas velocities extending from near bubbling right up into fast fluidization conditions. Other ozone decomposition data in the literature are either for cases where P_{fast} is close to 0, so that they do not provide a test of the fast fluidization upper end of the spectrum added in this article, or they solely pertain to cases where P_{fast} is essentially 1 (such as data of Ouyang and Potter (1995)) where the model reduces to the simple core-annulus model. The particle properties and operating conditions employed in the investigation are shown in Table 4. The velocity range covers bubbling, turbulent and fast fluidization flow regimes (with $U_c = 0.55$ m/s and $U_{se} = 1.38$ m/s, respectively, estimated from the correlations in Table 2). Other considerations in applying the model to these data are:

(a) The ozone decomposition reaction was conducted at atmospheric conditions with a very small inlet concentration of ozone. Also, the column is shallow enough ($L_t = 2$ m) that pressure gradients are not very significant. Therefore, it is assumed that both temperature and pressure variations along the column height and volume changes due to reaction are negligible.

Table 3. Summary of Regime Bounds and Transition Equations

Variables/ Parameters, θ	Regime-Specific Parameter Values, θ_j j = Bubbling	j = Turbulent	j = Fast Fluidization
ϵ	$\dfrac{1-(1-\epsilon_{mf})}{\left(1+\dfrac{U-U_{mf}}{0.711\sqrt{gd_b}}\right)}$ (Clift and Grace, 1985)	$\dfrac{U+1}{U+2}$ (King, 1989)	$\left[1+\dfrac{G_{so}\Psi_{slip}}{\rho_p U}\right]^{-1}$ $^{++}$ (Patience et al., 1992)
$k_{LH}a_I$	$\left\{\dfrac{U_{mf}}{3}+2\left[\dfrac{D_{mix}\epsilon_{mf}u_{br}}{\pi d_b}\right]^{1/2}\right\}\times\dfrac{6}{d_b}$ (Sit and Grace, 1981)	$1.631Sc^{0.37}U$ (Foka et al., 1996)	$\left[\dfrac{4D_{mix}\bar{\epsilon}_a U}{\pi L_t}\right]^{1/2}\times\dfrac{2}{r_C}$ (Pugsley et al., 1992)
ψ_L	$(\epsilon-\epsilon_{mf})/(\epsilon_{L0}-\epsilon_{mf})$ {in limit $\epsilon_H\to\epsilon_{mf}$ & $\epsilon_L\to\epsilon_{L0}=(1-\phi_{Lo})$}		r_C^2/R^2
$D_{zg,L}$	D_{mix}	UL_d/Pe_{z1}*	$0.184\bar{\epsilon}_C^{(-4.445)}$
$D_{rg,L}$	$0.1\times D_{zg,L}$		
D_{zg}	UL_d/Pe_{z1}*	UL_d/Pe_{z1}*	UL_t/Pe_{z2} $^{+}$
$D_{rg,H}$	$0.1\times D_{zg,H}$		
u_L	$\text{MIN}(\epsilon_L u_{br}, (U-U_{mf})/\psi_L)$	U	U/ψ_C
ϕ_L	ϕ_{L0}	$1-\epsilon$	$1-\bar{\epsilon}_C$

Point estimate $\hat{\theta}$ in column 1 is obtained by weighting θ_j with P_j as: $\hat{\theta}=\sum_{j=1}^{3}\theta_j P_j$

*$Pe_{z1}=f_{Pe}\times 3.472\text{Ar}^{0.149}Re^{0.023}Sc^{-0.232}(L_d/D_t)^{0.285}$ (Bi et al., 2000).
+$Pe_{z2}=f_{Pe}\times UL_t/(0.184\bar{\epsilon}^{(-4.445)})$ (Li and Wu, 1991).
++$\Psi_{\text{slip}}=1+5.6/Fr^2+0.47Fr_t^{0.41}$ (Patience et al., 1992).

(b) Sun (1991) estimated that about 20% of the solids were in the solids return system during the experiments. Hence, the solids inventory was adjusted in all cases so that $M_s=0.8\times M_{so}$.

(c) The voidage at minimum fluidization ϵ_{mf} was taken as 0.48 from Grace and Sun (1991).

(d) Three parameters appearing in the transition equations (Table 3) needed to predict the limiting conditions in the GFBR model, one per flow regime, were fitted using one of the three sets of data from the study of Sun (1991), the only published study which spans all three flow regimes under consideration:

(i) The initial volume fraction ϕ_{Lo} of solids in the L-phase at the lowest superficial velocity was estimated to be 0.0355 by matching model predictions with data at the lowest U values, using the two-phase bubbling bed model. This value is consistent with the finding that particles typically occupy a few percent of the bubble phase for group A particles.

Table 4. Operating Conditions, Hydrodynamic Properties and Reactor Geometry (Details are Given by Sun (1991))

Parameter	Value
Inlet temperature, T_o	298 K
Inlet pressure, P_o	101 kPa
Inlet superficial gas velocity, U_o	Varied (0.1 to 1.75 m/s)
Expanded bed height, L_d	Varied (~ 0.56 to 2.0 m)
Average particle diameter, $\bar{d}_p$	60 μm
Initial solids inventory, M_{so}	5 kg
Catalyst density, ρ_p	1,580 kg/m^3
Catalyst rate constant, k_r	Varied (8.95, 4.62 and 2.41 s^{-1})
Inside diameter of reactor, D_t	0.105 m
Column overall height, L_t	2.0 m

(ii) The average solids flux under fast fluidization conditions G_{so} was estimated to be 120 kg/m^{2}s by matching model predictions with data using the GFBR model for intermediate velocities ($1.4<U<1.8$ m/s) between turbulent and fast fluidization conditions. There are no precedents for this parameter, but the fitted value is of a reasonable order of magnitude with respect to fluxes encountered in studies of fast fluidization.

(iii) Axial dispersion correlations for the turbulent flow regime of fluidization differ by orders of magnitude (Bi et al., 2000) as for the entire fluidization spectrum. The f_{Pe} parameter was chosen to be 0.0711 with the single-phase axial dispersion model fitted to reactor results pertaining to the turbulent flow regime. The resulting Peclet numbers are of order 1, well within the range of experimentally determined values.

After these three values were chosen based on one of the Sun (1991) sets of data, they were held constant and applied to the other Sun data sets. The purpose of the article is to test a reactor model, and this approach reduces the probability that uncertainty in specifying *hydrodynamic* parameters could spoil the quantitative agreement between the *reactor* model and available reactor results.

Results and Discussion

Hydrodynamics

Figure 4 shows exponential decay of solids holdup in the freeboard according to Eq. 13 for different gas velocities and the other conditions given in Table 4. As expected, at low gas velocities ($U=0.03$ m/s $=5\times U_{mb}$), the model predicts only a

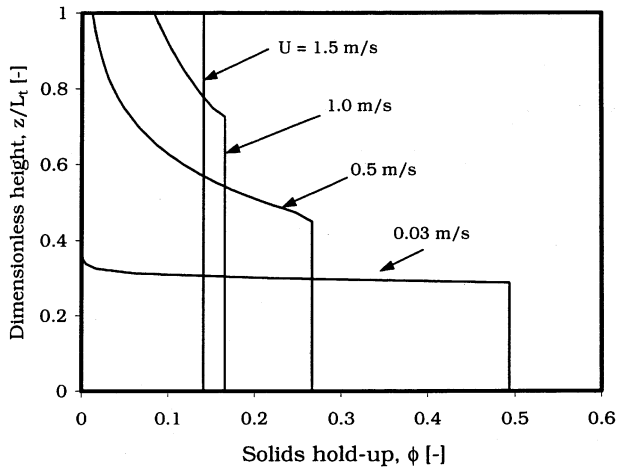

Figure 4. Axial profiles of solids holdup in column at different superficial gas velocities.

Conditions are listed in Table 4.

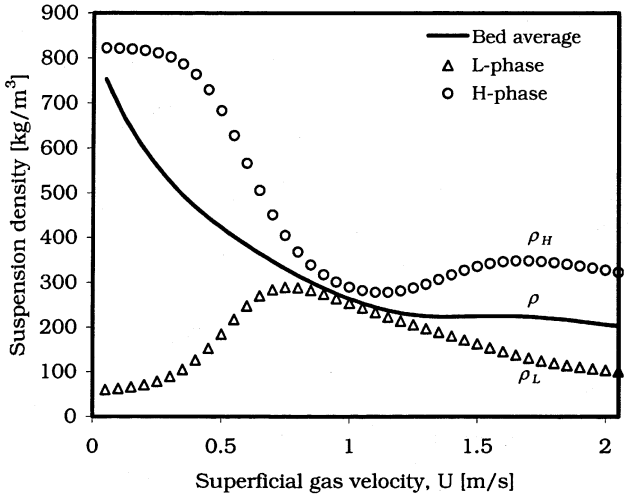

Figure 6. Predicted suspension densities in low- and high-density phases and bed average with increasing superficial gas velocity in the dense bed.

Conditions are listed in Table 4.

small fraction of solids in the freeboard. Solids holdup in the freeboard is predicted to increase with increasing gas velocity, while the column-average value decreases. The height at which the decay starts corresponds to the dense bed height L_d. The predicted solids holdup at $U \cong 1.5$ m/s $> U_{se}$ indicates that L_d approached the total column height ($L_t = 2$ m). Solids holdup from then on becomes a strong function of the net solids flux.

Figures 5 and 6 show predicted phase and average gas velocities and densities with increasing superficial gas velocity for the ozone decomposition reactor operated by Sun (1991) whose operating conditions appear in Table 4. The phases are quite distinct at low velocities where the L (low-density) phase accommodates most of the gas flow, while the H (dense) phase, composed of solids and interstitial gas, occupies most of the volume. Hence, as seen in Figure 5, u_H trails u_L, as almost all the excess gas flow $(U\text{-}U_{mf})A$ passes via the low-density phase. As U increases, however, the two phases merge, that is, become almost identical, corresponding to the nearly homogeneous behavior encountered within the turbulent fluidization flow regime. As U increases further, the bed begins to segregate into a continuous dilute core surrounded by a dense annular region as fast fluidization gradually takes over. For the core-annulus model, it is assumed, in the fast fluidization limit, that gas flows upward in the core only, with zero net flow of gas in the annulus. Thus, u_H is seen to approach zero, while ρ_L approaches a low value equivalent to $\rho_p \times \phi_L$, with ϕ_L being the dilute phase solids concentration.

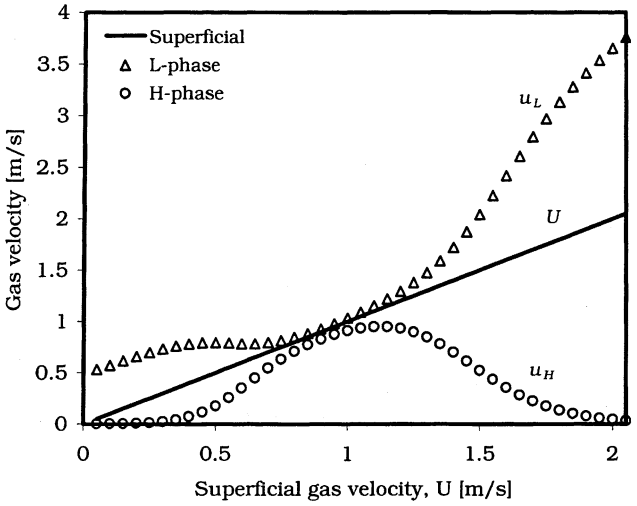

Figure 5. Predicted gas velocities in low- and high-density phases and bed average with increasing superficial gas velocity in the dense bed.

Conditions are listed in Table 4.

Reactor performance

(a) Influence of Freeboard on Ozone Conversion. Figure 7 shows the dense bed height predicted based on Eq. 19 as a function of increasing gas velocity, both with the freeboard included and ignored. With the freeboard ignored, the expanded bed height is computed by assigning all the solids to the dense region. A smaller expansion is predicted when the freeboard is included, because some of the particles are dispersed there. When U is high enough, the predicted bed heights in both cases reach the column height L_t.

Figure 8 shows predicted axial profiles of ozone conversion at different gas velocities for the two same cases. For low and intermediate U, solids dispersed in the freeboard are more effective in catalyzing the reactions than additional particles in the bed, where the bubble-to-dense phase mass-transfer resistance is appreciable. However, when U is high enough that the bed expands to fill the entire column, there is no difference in the predictions for the two cases.

The performance of the GFBR model, with and without the freeboard considered, is tested by comparing model predictions with experimental data over a wide range of superficial gas velocities and catalyst activities in Figure 9. Inclusion

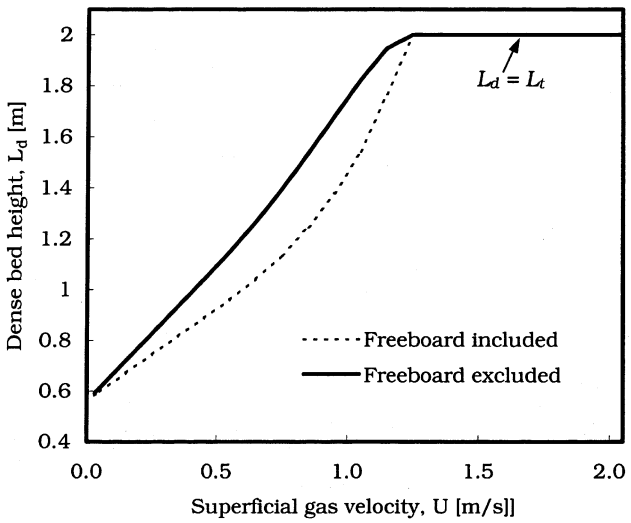

Figure 7. Comparison of computed expanded bed height when freeboard is included in GBR model and when it is ignored.

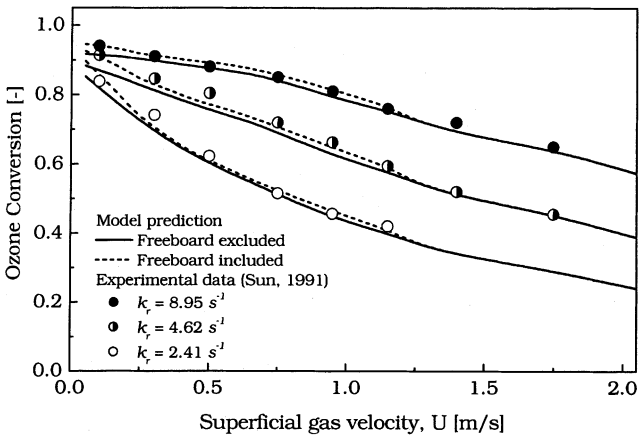

Figure 9. Comparison of predicted ozone conversions with experimental data for different catalyst activities when the freeboard is included in the GFBR model and when it is excluded.

of the freeboard appears to give somewhat better agreement with the data. For $U > 1.2$ m/s, predictions from the two cases merge as explained above. Overall, the freeboard is important when its height occupies a significant fraction of the total column height. For highly exothermic reactions, the dense region provides good temperature control (because of intense solids mixing and circulation), while the freeboard can be subject to large temperature variations. Further reactions in the freeboard can profoundly change the final species compositions, especially for complex reactions where selectivity is important.

(b) Comparison of Predictions from Regime-Specific and Probabilistic Models. Figure 10 compares predictions from the three individual regime-specific models—generalized two-phase bubbling bed at low U, dispersed flow at intermediate U, and generalized core-annulus at high U—with the experimental ozone decomposition data of Sun (1991). Sharp transitions at the U_c and U_{se} boundaries cause discontinuities in the predicted conversions when the three separate regime-specific models are employed. Such discontinuities are not observed experimentally. The *GFBR* model correctly predicts a smooth transition in the conversion (as well as other variables) as one spans the flow regimes. It also gives improved agreement with the experimental data as shown in Figure 10.

Conclusions

A new generic fluid-bed reactor model is presented which interpolates between three regime-specific models by probabilistic averaging of hydrodynamic and dispersion variables based on the uncertainty in the flow regime transitions. Predictions of hydrodynamic variables across the fluidization flow regimes most commonly encountered in industrial scale fluid-

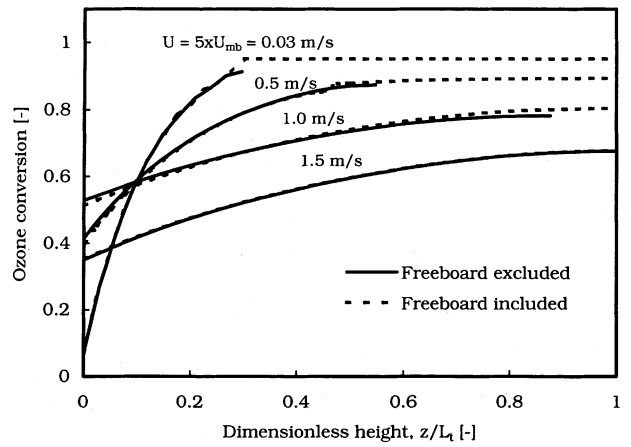

Figure 8. Predicted axial ozone conversions with the freeboard included in the GFBR model and with it excluded at different superficial gas velocities ($k_r = 8.95$ s^{-1}).

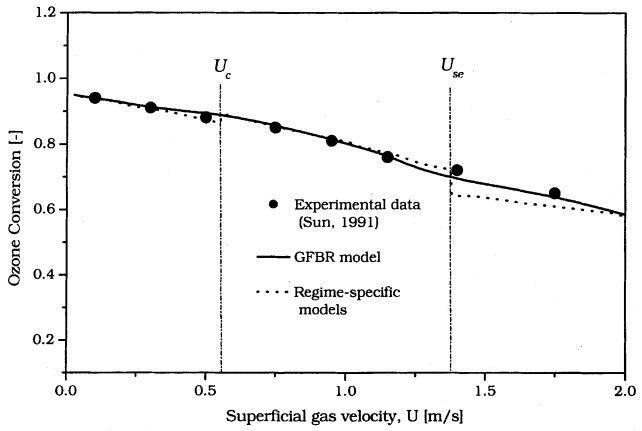

Figure 10. Predicted and experimental conversion trends.

(a) Individual regime-specific models which switch sharply at regime boundaries; (b) GFBR model. $k_r = 8.95$ s^{-1}. Other conditions are given in Table 4.

bed reactors—bubbling, turbulent, and fast fluidization—are realistic, while conversion predictions are in good agreement with available experimental data. This approach leads to improved predictions of reactor performance compared with any of the three separate models for individual flow regimes, while avoiding discontinuities at the boundaries between the flow regimes. The contribution of the freeboard is shown to be important for reactors where bubbling plays a strong role, especially where the freeboard height represents a significant fraction of total column height. This approach has been successfully validated with two industrial catalytic gas-solid processes—oxy-chlorination of ethylene and oxidation of naphthalene to phthalic anhydride (Abba, 2001; Abba et al., 2002).

Notation

a_I = interphase transfer surface area per unit volume of gas in low-density phase, m^{-1}
A = bed cross-sectional area, m^2
Ar = Archimedes number, $\rho_g(\rho_p - \rho_g)g\bar{d}_p^3/\mu^2$
A_s = heat-transfer surface area per unit reactor volume, m^{-1}
C_i = concentration of species i, mol/m^3
$C_{i,L}$; $C_{i,H}$ = concentration of species i in L-phase, H-phase, mol/m^3
C_{pg} = specific heat of gas, J/mol K
d_b = volume-equivalent bubble diameter, m
$\bar{d}_p$ = mean particle diameter, m
D = molecular diffusivity of gas, m^2/s
D_{mix} = mixture diffusivity, m^2/s
D_t = column/reactor diameter, m
$D_{z,g}$ = axial gas dispersion coefficient, m^2/s
$D_{r,g}$ = radial gas dispersion coefficient, m^2/s
E = error or uncertainty in regime boundary estimation, m/s
f_{pe} = parameter used to adjust Peclet number (Table 3)
Fr = Froude number based on U, $U/\sqrt{gD_t}$
Fr_t = Froude number based on v_t, $v_t/\sqrt{gD_t}$
g = gravitational acceleration, m/s^2
G_{so} = average solids flux under fast fluidization conditions, kg/m^2s
G_s = net solids circulation flux, kg/m^2s
h = overall bed-to-surface heat-transfer coefficient, $W/m^2 \cdot K$
H = hypothesis (such as bubbling, turbulent, fast fluidization regime)
ΔH_k = heat of reaction k, kJ/kmol
k_e = effective axial thermal conductivity of solids, $W/m \cdot K$
k_{LH} = gas interchange coefficient between L and H phases, m/s
k_r = first-order reaction rate constant, s^{-1}
K = interphase volumetric mass-transfer coefficient, s^{-1}
L = column height at any level, m
L_d = dense bed height, m
L_f = freeboard height, m
L_t = total column height, m
M_s = solids inventory, kg
N_g = number of gaseous components
N_r = number of reactions
P = pressure, kPa
P_j = probability of being in regime j
P_o = inlet pressure, kPa
$p(.)$ = probability density function (pdf), s/m
$p(.|.)$ = conditional probability density function
Pe_z = Peclet number, UL_d/D_{zg}
Pe_{z1} = Peclet number based on L_d, UL_d/D_{zg}
Pe_{z2} = Peclet number based on L_t, UL_t/D_{zg}
q_i = fraction of total flow passing through phase i
Q = gas-flow rate, m^3/s
r = radial coordinate, m
r_C = core radius, m
r_k = rate expression for reaction k, kmol/kg s
R = column radius, m
Re_c = Reynolds number based on U_c, $\rho_g U_c \bar{d}_p/\mu$
Re_p = particle Reynolds number, $\rho_g U \bar{d}_p/\mu$
Re_{se} = Reynolds number based on U_{se}, $\rho_g U_{se} \bar{d}_p/\mu$
T = reactor temperature, K
T_{cool} = coolant temperature, K
T_o = inlet temperature, K
u_{br} = bubble rise velocity, m/s
u_j = absolute gas velocity in phase j, m/s
U = superficial velocity of gas at any level, m/s
U^* = dimensionless superficial gas velocity, $U[\rho_g^2/\mu g(\rho_p - \rho_g)]^{1/3}$
U_c = transition velocity from bubbling to turbulent fluidization, m/s
U_i = transition velocity to regime i, m/s
U_{DSU} = onset of dense suspension upflow, m/s
U_{se} = transition gas superficial velocity to fast fluidization regime, corresponding to significant solids entrainment, m/s
v_c^* = normalized transition velocity from bubbling to turbulent fluidization (Eq. 28)
v_{se}^* = normalized transition velocity to fast fluidization regime, corresponding to significant solids entrainment (Eq. 29)
v_t = terminal settling velocity of particles, m/s
x = any hydrodynamic variable (such as k_q, ψ_L, $D_{zg,L}$)
y = set of performance variables (such as conversion, selectivities)
z = axial coordinate, positive upwards, measured from grid, m
z_f = axial coordinate in freeboard (Figure 1), m

Greek letters

β = fitting parameter in logistic regression function
ϵ = voidage
$\bar{\epsilon}$ = cross-sectional average voidage
θ = set of operating conditions and physical properties (such as T_o, P_o, ρ_g)
ν = stoichiometric coefficient
μ = absolute viscosity of gas, kg/m s
ρ = density, kg/m^3
σ = standard deviation of uncertainty in regime boundary correlation, m/s
ϕ = solids volume fraction
ϕ^* = saturation carrying capacity
ψ = phase volume fraction
Ψ_{slip} = slip factor $= 1 + 5.6/Fr^2 + 0.47Fr_t^{0.41}$

Subscripts

a = annular (outer) region
b = bubble phase or bubble
bubb = bubbling flow regime
c = critical
C = core region
CA = type A (accumulative) choking
d = dense phase
f = freeboard
fast = fast fluidization flow regime
g = gas
H = high density phase
L = low density phase
mb = minimum bubbling
mf = minimum fluidization
o = initial/inlet
p = particle
r = radial
s = surface
se = significant entrainment
t = total
turb = turbulent flow regime
z = axial

Superscript

$*$ = dimensionless variable

Literature Cited

Abba, I. A., "A Generalized Fluidized Bed Reactor Model across the Flow Regimes," PhD Thesis, University of British Columbia, Vancouver, Canada (2001).

Abba, I. A., J. R. Grace, and H. T. Bi, "Variable-Gas-Density Fluidized Bed Reactor Model for Catalytic Processes," *Chem. Eng. Sci.*, **57**, 4797 (2002).

Bi, H. T., "Flow Regime Transitions of Gas-Solid Fluidization and Transport," PhD Diss., University of British Columbia, Vancouver, Canada (1994).

Bi, H. T. and J. R. Grace, "Effect of Measurement Method on the Velocities Used to Demarcate the Onset of Turbulent Fluidization," *Chem. Eng. J.*, **57**, 261 (1995).

Bi, H. T., N. Ellis, I. A. Abba, and J. R. Grace, "A State-of-the-art Review of Gas-Solid Turbulent Fluidization," *Chem. Eng. Sci.*, **55**, 4789 (2000).

Bi, H. T., J. R. Grace, and J. Zhu, "Regime Transitions Affecting Gas-Solids Suspensions and Fluidized Beds," *Trans. IChemE*, **73**, 154 (1995).

Bolthrunis, C. O., "An Industrial Perspective on Fluid Bed Reactor Models," *Chem. Eng. Prog.*, 51 (May 1989).

Brereton, C. H. M., J. R. Grace, and J. Yu, "Axial Gas Mixing in Circulating Fluidized Bed," *Circulating Fluidized Bed Technology II*, P. Basu and J. F. Large, eds., Pergamon, Oxford, pp. 307–314 (1988).

Choi, J. H., H. J. Ryu, D. W. Shun, J. E. Son, and S. D. Kim, "Temperature Effect on the Particle Entrainment Rate in a Gas Fluidized Bed," *Ind. Eng. Chem. Res.*, **37**, 1130 (1998).

Clift, R., and J. R. Grace, "Continuous Bubbling and Slugging," *Fluidization*, 2nd ed., Chap. 3, J. F. Davidson, R. Clift, and D. Harrison, eds., Academic Press, London, pp. 73–132 (1985).

Edwards, M., and A. Avidan, "Conversion Model Aids Scale-Up of Mobil's Fluid Bed MTG Process," *Chem. Eng. Sci.*, **41**, 829 (1986).

Fane, A. G., and C. Y. Wen, "Fluidized Bed Reactors," *Handbook of Multiphase Systems*, Chap. 8.4, G. Hetsroni, ed., Hemisphere Publishing, Washington, DC (1982).

Foka, M., C. Chaouki, and C. Guy and D. Klavana, "Gas Phase Hydrodynamics of a Gas-Solid Turbulent Fluidized Bed Reactor," *Chem. Eng. Sci.*, **55**, 713 (1996).

Grace, J. R., "Generalized Models for Isothermal Fluidized Bed Reactors," *Recent Advances in the Engineering Analysis of Chemically Reacting Systems*, L. K. Doraiswamy, ed., Wiley, New Delhi, pp. 237–255 (1984).

Grace, J. R., I. A. Abba, H. T. Bi, and M. L. Thompson, "Fluidized Bed Catalytic Reactor Modeling across the Flow Regimes," *Can. J. Chem. Eng.*, **77**, 305 (1999).

Grace, J. R., and H. T. Bi, "Introduction to Circulating Fluidized Beds," *Circulating Fluidized Beds*, Chap. 1, J. R. Grace, A. A. Avidan, and T. M. Knowlton, eds., Chapman and Hall, London, p. 1 (1997).

Grace, J. R., A. S. Issangya, D. Bai, and H. T. Bi, "Situating the High-Density Circulating Fluidized Bed," *AIChE J.*, **45**, 2108 (1999).

Grace, J. R., and K. S. Lim, "Reactor Modeling for High-Velocity Fluidized Beds," *Circulating Fluidized Beds*, Chap. 15, J. R. Grace, A. A. Avidan, and T. M. Knowlton, eds., London, Chapman Hall, pp. 504–524 (1997).

Grace, J. R., and G. Sun, "Influence of Particle Size Distribution on the Performance of Fluidized Bed Reactors," *Can. J. Chem. Eng.*, **69**, 1126 (1991).

Han, I. S., and C. B. Chung, "Dynamic Modeling and Simulation of a Fluidized Catalytic Cracking Process. Part I: Process Modeling," *Chem. Eng. Sci.*, **56**, 1951 (2001).

King, D. F., "Estimation of Dense Bed Voidage in Fast and Slow Fluidized Beds of FCC Catalyst," *Fluidization VI*, J. R. Grace, L. W. Shemilt, and M. A. Bergougnou, eds., Engineering Foundation, New York, pp. 1–8 (1989).

Kunii, D., and O. Levenspiel, "Circulating Fluidized Bed Reactors," *Chem. Eng. Sci.*, **52**, 2471 (1997).

Kunii, D., and O. Levenspiel, *Fluidization Engineering*, 2nd ed., Butterworth-Heinemann, Stoneham, MA (1991).

Kunii, D., and O. Levenspiel, *Fluidization Engineering*, Wiley, New York (1969).

Lainiotis, D. G., "Optimal Adaptive Estimation: Structure and Parameter Adaptation," *IEEE Trans. Automat. Contr.*, **AC-16**, 160 (1971).

Li, T., and P. Wu, "A Study on Axial Gas Mixing in a Fast Fluidized Bed," *Circulating Fluidized Bed Technology III*, P. Basu, M. Horio, and M. Hasatani, eds., pp. 581–586 (1991).

Morikawa, H., H. T. Bi, C. J. Lim, and J. R. Grace, "Entrainment from Pilot Scale Turbulent Fluidized Beds of FCC Particles," *Fluidization X*, M. Kwauk, J. Li, and W. C. Yang, eds., pp. 181–188 (2001).

Murray-Smith, R., and T. A. Johanssen, eds., *Multiple Model Approaches to Nonlinear Modeling and Control*, Taylor and Frances, London (1997).

Ouyang, S., S. G. Li, and O. E. Potter, "Circulating Fluidized Bed as a Chemical Reactor: Experimental Study," *AIChE J.*, **41**, 1534 (1995).

Patience, G. S., J. Chaouki, F. Berruti, and R. Wong, "Scaling Considerations for Circulating Fluidized Bed Risers," *Powder Tech.*, **72**, 31 (1992).

Puchyr, D. M. J., A. K. Mehrotra, and L. A. Behie, "Modeling a Circulating Fluidized Bed Riser Reactor with Gas-Solids Downflow at the Wall," *Can. J. Chem. Eng.*, **75**, 317 (1997).

Pugsley, T. S., G. S. Patience, F. Berruti, and J. Chaouki, "Modeling the Catalytic Oxidation of n-Butane to Maleic Anhydride Using a Circulating Fluidized Bed Reactor," *Ind. Eng. Chem. Res.*, **31**, 2652 (1992).

Rhodes, M., "What is Turbulent Fluidization?," *Powder Tech.*, **88**, 3 (1996).

Sit, S. P., and J. R. Grace, "Effect of Bubble Interaction on Interphase Mass Transfer in Gas Fluidized Beds," *Chem. Eng. Sci.*, **36**, 327 (1981).

Sun, G. L., "Influence of Particle Size Distribution on the Performance of Fluidized Bed Reactors," PhD Diss., University of British Columbia, Vancouver, Canada (1991).

Sun, G., and J. R. Grace, "Effect of Particle Size Distribution on the Performance of Fluidized Bed Reactors," *Chem. Eng. Sci.*, **45**, 2187 (1990).

Thompson, M. L., "Combining Prior Models and Nonparametric Models of Chemical Processes," PhD Thesis, Massachusetts Institute of Technology, Cambridge, MA (1996).

Thompson, M. L., H. T. Bi, and J. R. Grace, "A Generalized Bubbling/Turbulent Fluidized Bed Reactor Model," *Chem. Eng. Sci.*, **54**, 2175 (1999).

Manuscript received Sept. 13, 2001, and revision received Jan. 27, 2003.